Enhanced Performance of Organic Solar Cells with Increased End Group Dipole Moment in Indacenodithieno[3,2-b]thiophene-Based Molecules

*Jeremy J. Intemann, Kai Yao, Feizhi Ding, Yunxiang Xu, Xukai Xin, Xiaosong Li, and Alex K.-Y. Jen**

Four new molecular donors are reported using a D1-A-D2-A-D1 structure, where D1 is an oligiothiophene, A is a benzothiadiazole, and D2 is indacenodithieno[3,2-b]thiophene. The resulting materials provide efficiencies as high as 6.5% in organic solar cells, without the use of solvent additives or thermal/solvent annealing. A strong correlation between the end group (D1-A) dipole moment and the fill factor (FF), mobility, and loss in the open-circuit voltage (V_{OC}) is observed. Indacenodithieno[3,2-b]thiophene-fluorobenzothiadiazole-terthiophene (IDTT-FBT-3T) possesses the largest end group dipole moment, and in turn, has the highest mobility, FF, and power conversion efficiency in devices. It also has a similarly high V_{OC} (0.95 V) to the other materials (0.93–0.99 V), despite possessing a much higher highest occupied molecular orbital (HOMO) energy level.

1. Introduction

Research into organic photovoltaic cells (OPVs) that utilize a molecular electron donating semiconductor has gained considerable momentum the past few years as new insights into molecular design have given rise to materials with reported power conversion efficiencies (PCEs) of over 10% in single junction[1] and tandem cells.[2] This has elevated molecular semiconductors to a level that is highly competitive with their polymeric counter parts.[3] Compared to polymers, molecular donors are easier to obtain with very high purity and possess a monodisperse molecular weight, the latter of which creates less batch-to-batch variation in the material performance and allows for the study of structure–property relationships without variations in molecular weight and polydispersity influencing the results.[4] Presently, the performance of the top molecular donors depends heavily on their degree of semicrystallinity and requires solvent additives and postprocessing techniques, such as annealing, in order to control bulk heterojunction (BHJ) morphology.[5] This causes an increase in device fabrication complexity and reduces batch-to-batch cell reproducibility.

Molecular donors that are insensitive to processing conditions and that are less dependent on crystallinity for efficient charge transport are highly desirable and may be better suited for roll-to-roll device fabrication. Among polymeric donors, one strategy that has proven successful for producing both high device efficiencies and an insensitivity to processing conditions, is the use of fused ring ladder-type donor moieties, as the coplanar ladder-type structure provides high hole mobilities in BHJs, even in amporphous films.[6]

To this end, attempts have been made to incorporate the ladder-type indacenodithiophene (IDT) donor moiety into the structure of novel molecular donors, with the resulting materials indeed showing a general insensitivity to processing conditions.[7] However, these materials have exhibited very low fill factors (FF) in devices (0.35–0.48), likely resulting from poor morphology and charge transport in BHJs. Due to the low FF, IDT-based molecules have only achieved PCEs up to 4.7%, far lower than the 7.5% achieved by IDT-based polymers.[8]

Indacenodithieno[3,2-b]thiophene (IDTT) is an alternate ladder-type donor moiety that has performed exceptionally well in polymeric semiconductors.[6b,d,9] Its longer fused ring structure produces higher hole mobilities and extinction coefficients for improved light harvesting, compared to IDT in polymeric materials, while still maintaining a reasonably low sensitivity to processing conditions. We believed these features could be used to make IDTT-based molecular donors for high efficiency OPVs.

Herein, we report four new IDTT-based molecules utilizing a D1-A-D2-A-D1 type structure, where D1 is an alkyl oligiothiophene-based donor, A is a benzothiadiazole (BT) acceptor, and D2 is IDTT (**Scheme 1**). Because the out-of-plane side chains of IDTT disrupt π-stacking, we hypothesized that π-stacking would occur primarily at the ends of the molecule, and therefore, the nature of the D1-A portion (hereafter referred to as the end group) would have a substantial effect on the morphology

Dr. J. J. Intemann,[+] Dr. K. Yao, Dr. Y. Xu, Dr. X. Xin, Prof. A. K.-Y. Jen
Department of Materials Science and Engineering
University of Washington
Seattle, WA 98195, USA
E-mail: ajen@u.washington.edu
F. Ding, Prof. X. Li
Department of Chemistry
University of Washington
Seattle, WA 98195-1700, USA
[+]Present address: Department of Natural and Applied Sciences, University of Wisconsin-Green Bay, Green Bay, WI 54311, USA

DOI: 10.1002/adfm.201501600

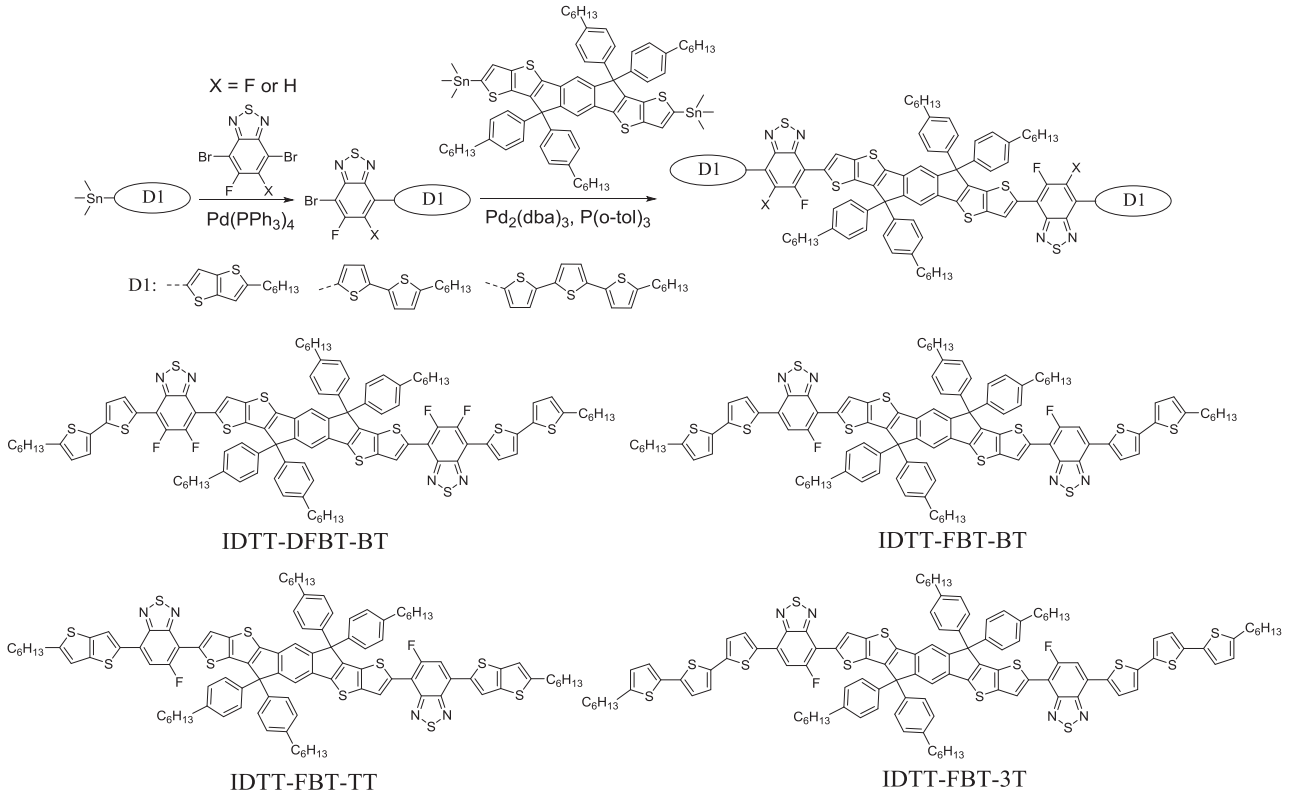

Scheme 1. Synthesis and structures of IDTT-based compounds.

and charge transport properties. In order to fine tune the electronic and aggregation properties of the materials, we varied the structure of the end group using two approaches. First, we used fluorine substitution on the BT unit by using 5-fluorobenzo[c][1,2,5]thiadiazole (FBT) or 5,6-difluorobenzo[c][1,2,5]thiadiazole (DFBT), in order to lower the HOMO/LUMO energy levels, increasing the open-circuit voltage (V_{OC}) of devices.[10] Increased fluorine substitution in the conjugated backbone is also known to increase π–π stacking.[11] Second, we used three different donors for D1, thieno[3,2-b]thiophene (TT), bithiophene (BT), and terthiophene (3T), which have increasing conjugation length and electron donating ability. We believed that increasing the conjugation length would lead to better π–π overlap between adjacent molecules in films, improving charge carrier mobilities, while the increased electron donating strength would decrease the optical band gap of the material, improving solar light absorption.

2. Results and Discussion

2.1. Material Synthesis and Characterization

The end groups were synthesized via a modified procedure previously reported by Bazan and co-workers[4a] and is outlined in Scheme 1. The Stille cross-coupling between 4,7-dibromo-5-fluorobenzo[c][1,2,5]thiadiazole and the corresponding alkyl oligiothiophenes is highly regioselective and the pure regio-specific products were confirmed by 2D NOESY NMR (Figures S1 and S2, Supporting Information). The resulting end groups were then coupled to IDTT via a second Stille cross-coupling reaction. The structures of the final molecules were confirmed by NMR and their purity was verified by elemental analysis and high resolution mass spectrometry (Figures S3–S6, Supporting Information). All four compounds possessed good solubility in common organic solvents such as dichloromethane, chloroform, and 1,2-dichlorobenzene.

The optical properties of the four new compounds were examined using UV–vis spectroscpy and their solution and film spectra are shown in **Figure 1**. The FBT-containing compounds show a general trend of red-shifting in absorption with increasing electron donating strength for D1, which increases from TT to BT to 3T. This increases the highest occupied molecular orbital (HOMO) energy level, reducing the optical band gap, and red-shifting absorption. IDTT-DFBT-BT has a slightly blue-shifted absorption compared to the less fluorinated IDTT-FBT-BT, which is a consequence of fluorine having a stronger stabilizing effect on the HOMO than on the lowest unoccupied molecular orbital (LUMO), resulting in a slight increase in the optical band gap.[10]

All four compounds have a noticeable red-shift between solution and film, indicative of strong intermolecular interactions from π-stacking. The redshift in the absorption onset between solution and film for IDTT-DFBT-BT, IDTT-FBT-TT, IDTT-FBT-BT, and IDTT-FBT-3T is 57, 45, 54, and 74 nm, respectively. This provides a qualitative measurement of the relative degree of π-stacking and aggregation for these compounds. Among the FBT molecules, not surprisingly, increasing the conjugation length causes a larger red-shift between the solution and

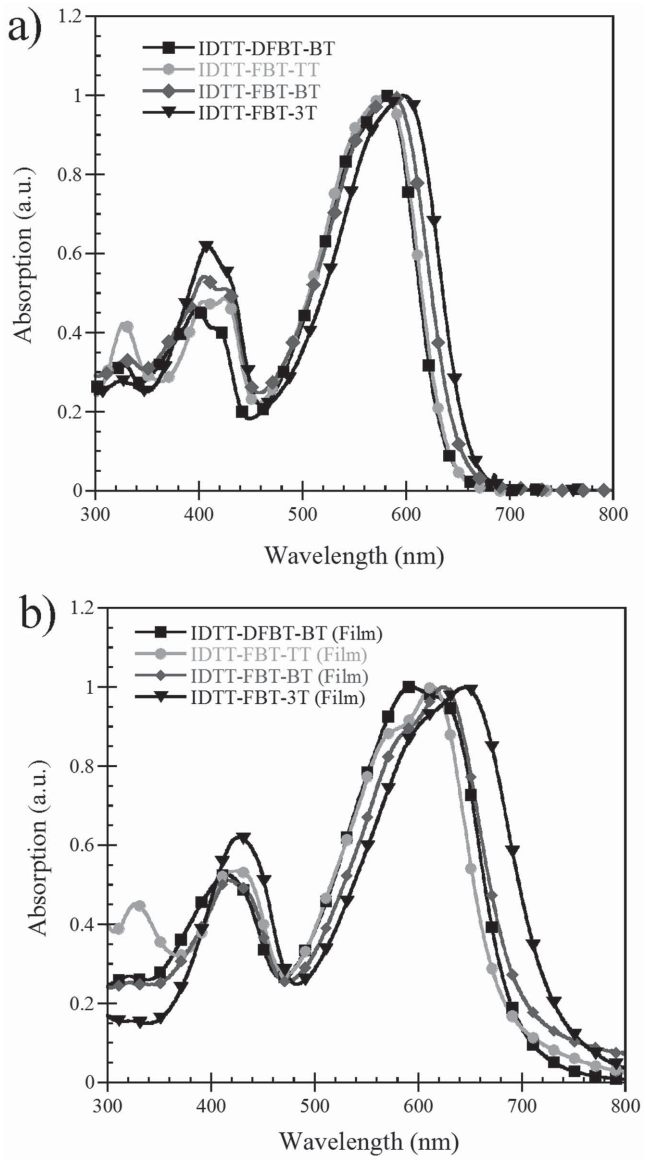

Figure 1. UV–vis absorption spectra of compounds in a) dilute chloroform solutions and b) thin films.

film spectra, due to stronger π-stacking. IDTT-DFBT-BT shows only a slightly larger red-shift compared to IDTT-FBT-BT, but not nearly as large of a red-shift as IDTT-FBT-3T. This suggests its tendency toward aggregation is similar to IDTT-FBT-BT but aggregates much less strongly than IDTT-FBT-3T. This is an important distinction that will be discussed below.

The frontier orbital energy levels of the materials were measured by cyclic voltammetry (Figure S7, Supporting Information) and are given in **Table 1**. All four of the molecules showed reversible oxidation cycles, though none exhibited good reduction properties. The HOMO energy was measured from the oxidation onset, while the LUMO was calculated using the HOMO energy level and the optical band gap. The FBT-based molecules all have the same LUMO energy level, differing only in their HOMO energy level. The HOMO level increases with increasing donor strength of the D1 moiety. IDTT-DFBT-BT has a slightly lower HOMO and LUMO energy levels than IDTT-FBT-BT due to the stabilizing effect of the extra fluorine atoms.

Table 1. Optical and electrochemical properties of IDTT-based compounds.

Compound	λ_{max}^{soln} [nm]	λ_{max}^{film} [nm]	$E_g^{opta)}$ [eV]	HOMO[b)] [eV]	LUMO[c)] [eV]
IDTT-DFBT-BT	580	594	1.78	−5.37	−3.59
IDTT-FBT-TT	580	614	1.82	−5.39	−3.57
IDTT-FBT-BT	587	624	1.77	−5.34	−3.57
IDTT-FBT-3T	598	645	1.69	−5.26	−3.57

[a)]Calculated from the absorption onset in films; [b)]Calculated from the oxidation onset of films using cyclic voltammetry; [c)]Calculated from the HOMO energy level and optical band gap.

2.2. Photovoltaic Devices

Photovoltaic devices were fabricated with the structure ITO/PEDOT:PSS/donor:$PC_{71}BM$/ Bis-C60/Ag, where ITO is indium tin oxide and PEDOT:PSS is poly(3,4-ethylenedioxythiophene)-poly(styrenesulfonate). The resulting *J–V* curves and external quantum efficiency (EQE) plots of optimized devices are displayed in **Figure 2**, and the results are summarized in **Table 2**. It was found that a 1:2 donor:$PC_{71}BM$ ratio gave the best performance, and that while IDTT-DFBT-BT exhibited optimum performance when annealed, the FBT-containing compounds performed best as unannealed as-spun films. Short-circuit current density (J_{SC}) increases with decreasing optical band gap of the materials, due to the improved solar spectrum coverage. This is not the case for IDTT-DFBT-BT; however, which has a lower J_{SC} than IDTT-FBT-BT, despite possessing a similar band gap to that of IDTT-FBT-BT. A high PCE of 6.5% was obtained from IDTT-FBT-3T without the need for solvent additives or postprocessing techniques, such as thermal or solvent annealing. Steadily increasing efficiencies with increasing conjugation length were observed in the FBT-containing compounds. Initially this was believed to be the result of increasing π–π overlap between molecules with increasing conjugation length, leading to improved charge transport and decreased recombination. This is reflected in increasing FF and EQE, which will be discussed further below.

Interestingly, IDTT-DFBT-BT exhibits the worst performance, despite possessing an identical conjugation length to IDTT-FBT-BT. Initially we speculated that the increased fluorine content was causing stronger aggregation in IDTT-DFBT-BT films, leading to unfavorably large phase domain sizes. Atomic force microscopy height images of IDTT-DFBT-BT and IDTT-FBT-BT seemed to confirm this (Figure S8, Supporting Information), with IDTT-DFBT-BT possessing much rougher surface features with a larger root mean squared roughness than IDTT-FBT-BT. However, as mentioned in the optical properties discussion, IDTT-DFBT-BT aggregates only slightly more strongly than IDTT-FBT-BT, and aggregates more weakly than IDTT-FBT-3T, yet IDTT-FBT-3T has superior performance. Additionally, the as-spun IDTT-DFBT-BT BHJ possesses smaller phase domains, yet unannealed devices gave a low PCE of 2.0%. So in IDTT-DFBT-BT's case, increasing the phase domain size improves

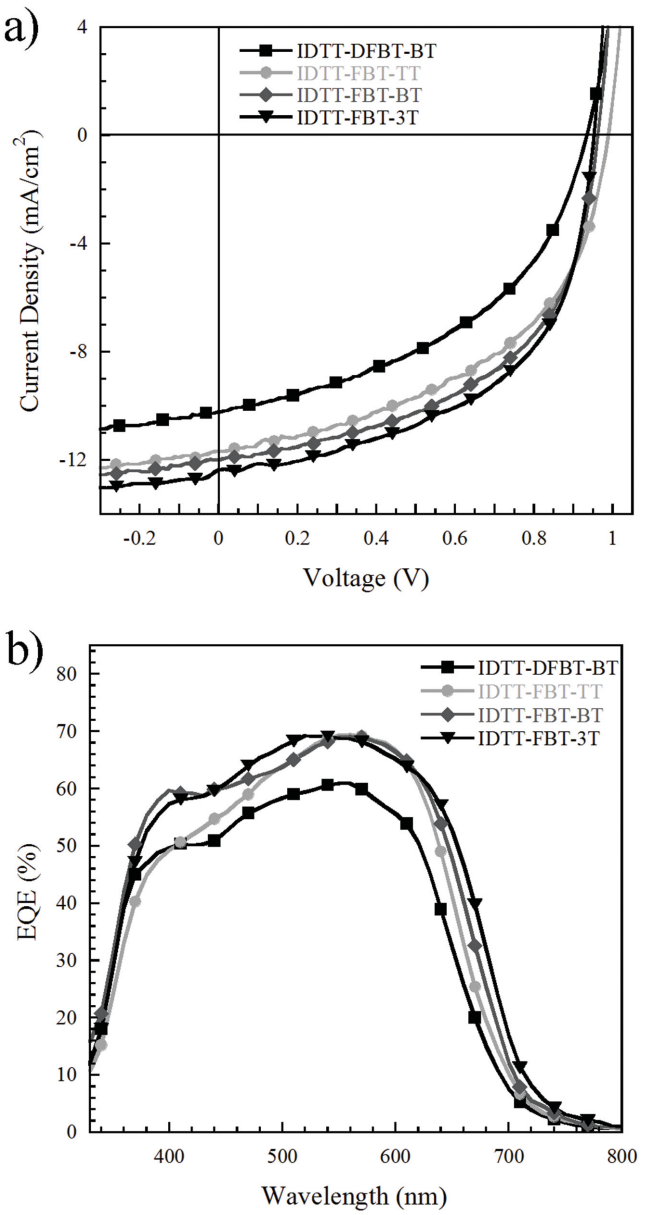

Figure 2. Characteristic a) current density–voltage (*J*–*V*) curves and b) external quantum efficiency (EQE) curves of BHJ solar cells under AM1.5G, 100 mW cm^{-2} illumination.

efficiency. This means there must be some other cause for the large difference in performance.

The changes seen in device efficiency are mainly due to differences in FF, as the J_{SC} and V_{OC} only fluctuate slightly. The differences in FF could be the result of differences in the charge transport properties of the BHJs. Mobilities in optimized BHJs were measured using the space-charge limited current (SCLC) model in hole-only and electron-only devices and the mobilities are listed in Table 2. There does seem to be some correlation between device FF and mobilities, with IDTT-DFBT-BT having the lowest hole mobility, and IDTT-FBT-3T possessing the highest, though it is not readily apparent why IDTT-DFBT-BT should have the lowest mobility. Furthermore, IDTT-FBT-TT and IDTT-FBT-BT have virtually identical hole mobilities and balance of hole and electron transport in devices, so the improvement in FF between IDTT-FBT-TT and IDTT-FBT-BT cannot be solely the result of differences in mobility.

Another interesting peculiarity lies in the V_{OC} of the devices. Despite having a lower HOMO energy level than either IDTT-FBT-BT or IDTT-FBT-3T, IDTT-DFBT-BT has the lowest V_{OC} in devices. This suggests that there is a voltage loss in the IDTT-DFBT-BT device. Theoretically, V_{OC} should be approximately equal to the difference in energy between the donor's HOMO and fullerene's LUMO energy level.[12] However, vacuum level misalignment,[12b,13] disorder-induced changes in the hole and electron quasi-Fermi levels,[14] poor dielectric properties,[15] and electronic coupling between the donor's ground state and the charge-transfer (CT) state[16] have been shown to cause losses in the V_{OC}.

We calculated the voltage loss in the V_{OC} (V_{loss}) for each material by subtracting the V_{OC} from the difference in energy between the donor's HOMO level and $PC_{71}BM$'s LUMO level (assuming a LUMO energy of ≈–4.2 eV).[17] The calculated V_{loss} for IDTT-DFBT-BT, IDTT-FBT-TT, IDTT-FBT-BT, and IDTT-FBT-3T was found to be 0.24, 0.20, 0.18, and 0.11 V, respectively. It is important to note that changes in V_{loss} do not follow the changes in the HOMO levels of the materials, eliminating vacuum level misalignment as the main source for the voltage loss. The calculated V_{loss} values, on the other hand, do follow the trend in FF, which suggests the voltage loss may be tied to charge recombination in the devices.

2.3. Consideration of Electrostatic Interactions

It has been proposed that the dipole moment of donor molecules strongly influences molecular self-assembly in films

Table 2. Photovoltaic and charge transport properties of optimized devices.

Compound[a)]	V_{OC} [V]	J_{SC} [mA cm^{-2}]	FF	PCE[b)] [%]	μ_h[c)] [cm^2 V^{-1} s^{-1}]	μ_e[c)] [cm^2 V^{-1} s^{-1}]
IDTT-DFBT-BT[d)]	0.93	10.0	0.46	4.37 (4.19 ± 0.12)	2.8×10^{-5}	5.1×10^{-5}
IDTT-FBT-TT[e)]	0.99	11.7	0.50	5.75 (5.56 ± 0.15)	2.1×10^{-4}	2.5×10^{-4}
IDTT-FBT-BT[e)]	0.96	12.0	0.53	6.12 (5.89 ± 0.18)	2.3×10^{-4}	2.6×10^{-4}
IDTT-FBT-3T[e)]	0.95	12.4	0.55	6.54 (6.40 ± 0.10)	7.5×10^{-4}	5.5×10^{-4}

[a)]Devices using a 1:2 donor:PC71BM ratio; [b)]Best efficiencies with average PCE over six devices in parantheses; [c)]Mobilities of electron and hole-only BHJ devices using the SCLC model; [d)]BHJ annealed at 110 °C for 10 min; [e)]As-spun films with no annealing.

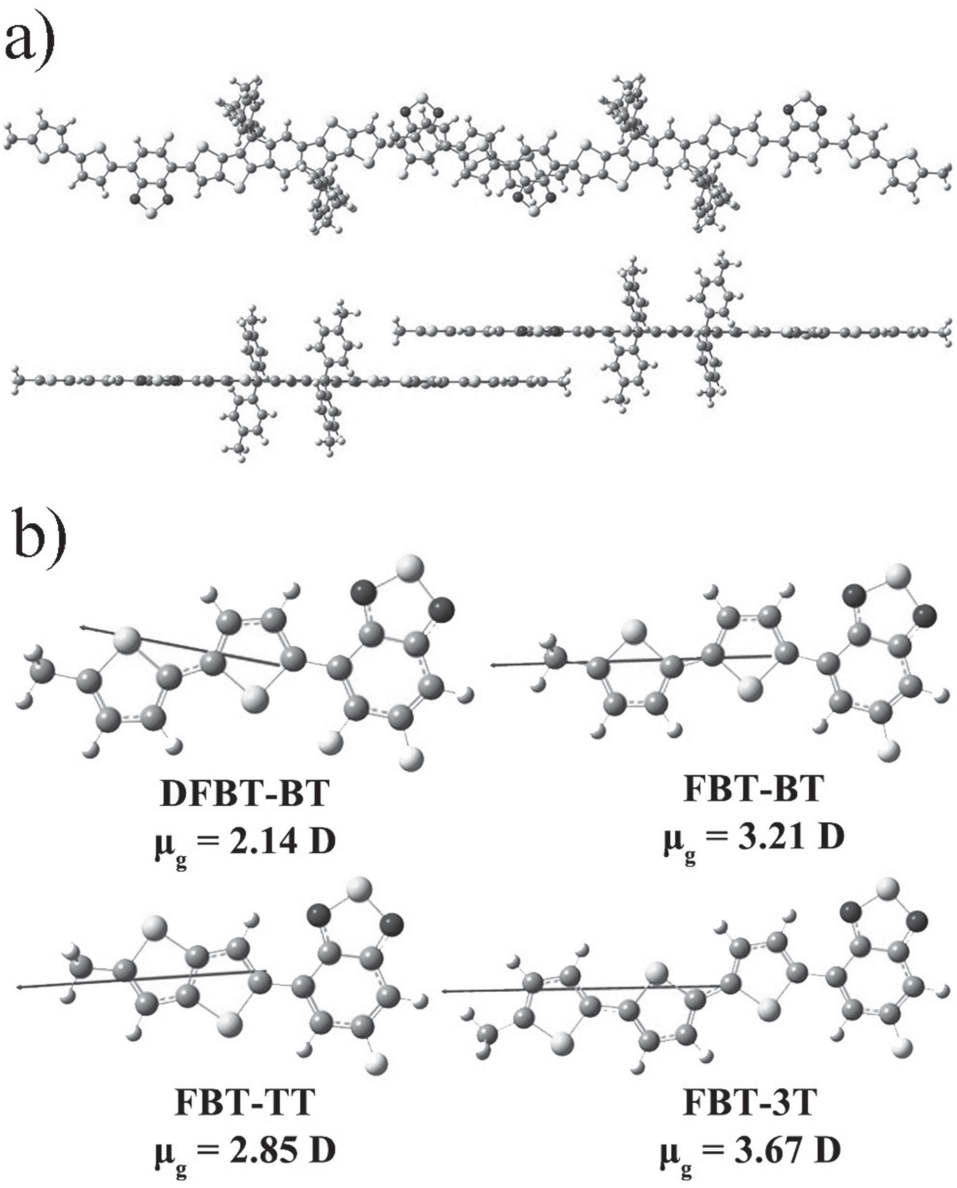

Figure 3. DFT-calculated optimized geometry of the proposed packing of a) two IDTT-FBT-BT molecules and b) ground-state dipole moments of the different end groups.

and the resulting morphology, as dipoles of adjacent molecules can align antiparallel to each other, inducing self-assembly and improving order and crystallinity in BHJ films.[18] Unlike other molecular donors, IDTT-based materials lack a high degree of crystallinity, due to the poor π-stacking ability of the IDTT moiety. As a result, we were unable to grow single crystals of the compounds and X-ray diffraction (XRD) experiments on thin films revealed only lamellar packing of the molecules with d-spacings of 1.2–1.5 nm (Figure S10, Supporting Information), so we were unable to probe the degree of nanoscale order in the films from π-stacking.

Due to IDTT's propensity to disrupt π-stacking, we believed that π-stacking interactions would occur predominantly at the ends of the molecules, away from the out-of-plane hexylphenyl side chains. **Figure 3**a shows the density functional theory (DFT) calculated optimized geometry of the proposed packing method of two IDTT-FBT-BT molecules. Based on this arrangement, it stands to reason that only localized dipoles at the ends of the molecules could aid in self-assembly. Quantum chemical calculations of the end group ground-state dipole moments (Figure 3b) yielded magnitudes of 2.14, 2.85, 3.21, and 3.67 D for DFBT-BT, FBT-TT, FBT-BT, and FBT-3T, respectively. From these results, several interesting trends now emerge from the empirical data. SCLC mobilities in devices increase with increasing dipole strength. If the molecules are packing at their ends, an increased dipole would result in increased self-assembly of molecules in this configuration, making longer supramolecular chains and providing improved percolation

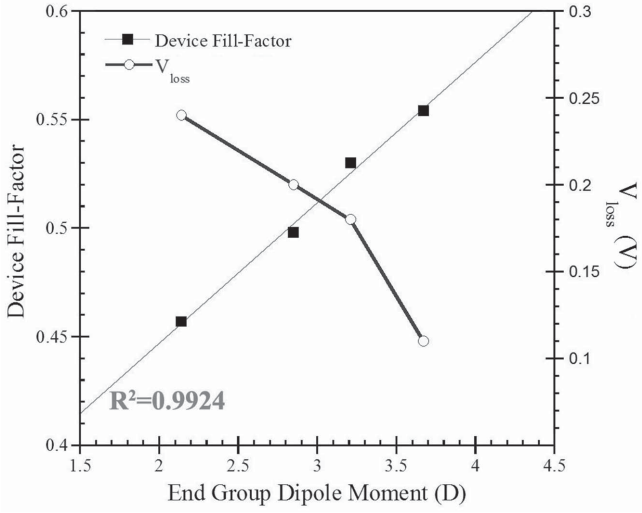

Figure 4. Plot of device FF and V_{loss} as a function of end group ground-state dipole moment.

pathways for charge carriers. Furthermore, **Figure 4** shows an astonishingly good linear correlation between the dipole moment of the end group and the FF of the devices, with a very high R^2 value of 0.9924 for the linear fit. Figure 4 also shows a very good inverse relationship between the end group dipole moment and V_{loss}. It is worth noting that the trends in FF and V_{loss} do not appear to be greatly influenced by the direction of the end group dipole moment. DFBT-BT, FBT-TT, FBT-BT, and FBT-3T possess dipole moments that are 1°, 10°, 17°, and 8° off-axis from the linear portion of the molecules and the dipole angles do not follow the same trends in device performance as the magnitudes.

We speculated that the increasing dipole strength may be resulting in increased self-assembly, causing a higher degree of order at the donor–acceptor interface, reducing the number of disorder-induced trap states, which would decrease charge recombination and increase FF.[19] Increased order at the donor–acceptor interface could also lead to a change in the density of states for holes and electrons, so that disorder-induced gap tail states are reduced, increasing the electron quasi-Fermi level and decreasing the hole qausi-Fermi level, increasing V_{OC}.[13b,20] This hypothesis seems to fit the observed losses in the open-circuit voltages, as the changes in V_{loss} are within the range expected for disorder-induced gap tail states (0.1–0.2 eV),[21] while effects from CT-state coupling are known to cause significantly larger changes in the V_{OC}.[16c]

Transmission electron microscopy (TEM) was used to examine the bulk-heterojunction films of the molecules for evidence of self-assembly and improved order. The TEM images can be seen in Figure S11 (Supporting Information). Unfortunately, due to the amorphous nature of the IDTT-based molecules, and the low difference in density between the molecules and [6,6]-phenyl C71 butyric acid methyl ester (PCBM), we were unable to see clear molecule-fullerene domains and there was no evidence of ordered nanostructures in the films. It may be that the end group dipole is directing the molecules to self-assemble into a 1D supramolecular polymer, which could be amorphous relative to the other supramolecular chains, making the improve order unobservable with either XRD or TEM.

Another possibility, as mentioned previously, is that the end group dipoles are enhancing the dielectric properties of the materials, which would decrease charge recombination (increasing FF and mobility) as well as the exciton binding energy of charges in the charge-transfer state (decreasing voltage loss) via shielding of charges by the surrounding dielectric environment. This possibility is interesting, as both our group and others have reported that doping active layers with polar materials[22] or adding polar side chains[23] to the donor semiconductor can enhance the dielectric properties of the BHJ. The polar groups help to shield holes and electrons from each other, inhibiting their coulombic attraction and decreasing charge recombination of either charge-transfer pairs or free charge carriers. These reports include improved FF as well as V_{OC} increases of ≈0.1 V from materials with polar side chains, which is similar to the changes in V_{loss} reported here. Further investigation is required to determine if this is indeed the reason behind the improved performance of the materials.

In order to evaluate our theory of the end group dipole effect on FF, we compared our results with another molecular donor reported in the literature by Hou and co-workers[7] IDT(BTTh$_2$)$_2$ has a very similar structure to that of IDTT-FBT-BT, except that it is lacking any fluorine substitution and the IDT core contains only a single fused thiophene at its ends, as opposed to the fused thienothiophene in IDTT. We calculated a dipole moment of 2.57 D for the end group of IDT(BTTh$_2$)$_2$. The linear fit found for the IDTT-based materials predicts a FF of 0.484, which is virtually identical to the FF of 0.485 reported for this material, suggesting that the end group dipole moment may play a more prominent role in determining the FF than the nature of the ladder-type core donor (D2) in these types of materials.

3. Conclusion

We have reported the synthesis of four new IDTT-based molecular donors that possess end groups of varied dipole strength and evaluated their performance in OPVs. A very good correlation between end group dipole strength and several device parameters, such as FF, mobility, and loss in the V_{OC} was observed. Several possible reasons for these observations were considered, including enhanced dielectric properties of the materials and increased order at the donor/acceptor interface. The best performance (6.5% PCE) was achieved by IDTT-FBT-3T, the molecule that possessed the highest end group dipole moment. These results illustrate a potential new design rule for improving device performance via the tuning of electrostatic interactions in molecular donors.

4. Experimental Section

Materials and Characterization: 7-Bromo-6-fluoro-4-(5′-hexyl-[2,2′-bithiophen]-5-yl)benzo[c][1,2,5]thiadiazole,[4a] 4,7-dibromo-5-fluorobenzo[c][1,2,5]thiadiazole,[4a] 4,7-dibromo-5,6-difluorobenzo[c][1,2,5] thiadiazole,[10] 6,6,12,12-tetrakis(4-hexylphenyl)-s-indacenodithieno[3,2-b]thiophene-bis(trimethylstannane),[9a] 5′-hexyl-2,2′-bithiophene-5-trimethylstannane,[24] (5″-hexyl[2,2′:5′,2″-terthiophen]-5-yl)trimethylstannane,[25] and trimethyl(5-hexylthieno[3,2-b]thien-2-yl)

stannane[26] were made according to literature procedures. 7-Bromo-6-fluoro-4-(5′-hexyl-[2,2′-bithiophen]-5-yl)benzo[c][1,2,5]thiadiazole was further purified after column chromatography by recrystallization in absolute ethanol to remove residual benzothiadiazole starting material. All other reagents were purchased from Aldrich and used without further purification. UV–vis spectra were measured using a Perkin-Elmer Lambda-9 spectrophotometer. The ^{1}H and ^{13}C NMR spectra were collected on a Bruker AV300 (operating at 300 and 75 MHz for ^{1}H and ^{13}C nuclei, respectively) and AV500 (operating at 500 and 125 MHz for ^{1}H and ^{13}C nuclei, respectively) spectrometers in deuterated chloroform solutions referenced to tetramethylsilane. Cyclic voltammetry of drop-cast films was conducted in a 0.1 M tetrabutylammonium hexafluorophosphate solution in acetonitrile, using a scan rate of 100 mV s^{-1}. Pt button, Ag/AgCl, and Pt mesh were used as the working electrode, reference electrode, and counter electrode, respectively. High-resolution mass spectroscopy (HRMS) measurements were performed on a Bruker Apex-Qe Fourier transform ion cyclotron resonance mass spectrometer with electrospray ionization (ESI) from the Medicinal Chemistry Department at the University of Washington. XRD patterns were recorded on a Bruker F8 Focus Powder XRD using drop-cast films on a glass substrate. Transmission electron microscopy images of bulk-heterojunction films were recorded on a FEI Tecnai G2 F20 transmission electron microscope operating at an acceleration voltage of 200 kV. All DFT calculations were performed using the Guassian 09 program package. To simplify computations, hexyl chains on the molecules were replaced with methyl groups.

SCLC Measurements: Space charge limited currents have been tested in electron-only devices with a configuration of ITO/Al/polymer:PCBM/Ca/Al and hole-only devices with a configuration of ITO/PEDOT:PSS/polymer:PCBM/Pd. The devices were prepared following the same procedure described in experimental section for photovoltaic devices, except that the metal electrode was replaced by palladium (50 nm). The dark current of the SCLC devices was measured under ambient by using an Agilent 4155B semiconductor parameter analyzer. The mobilities were determined by fitting the dark current to the model of a single carrier SCL current with field dependent mobility, which is described as

$$J = \frac{9}{8}\varepsilon_0\varepsilon_r\mu_0 \exp\left(0.891\gamma\sqrt{\frac{V}{L}}\right)\frac{V^2}{L^3}$$

where J is the current, μ_0 is the zero-field mobility, γ is the field activation factor, ε_o is the permittivity of free space, ε_r is the relative permittivity of the material, V is the effective voltage, and L is the thickness of the active layer. In simulation, ε_r was assumed to be 3 for hole-only devices and 4.5 for electron-only devices, which is a typical value for organic materials and fullerene. The effective voltage can be obtained by subtracting the built-in voltage (V_{BI}) and the voltage drop (V_{RS}) from the substrate's series resistance from the applied voltage (V_{APPL}), $V = V_{APPL} - V_{BI} - V_{RS}$. V_{BI} values of 0 and 0.5 V were used for electron-only and hole-only devices, respectively, which provided best fits to the log(J)–log(V) curves. The series resistance to our substrates was determined from the reference device without the active layer, i.e., a device configuration of ITO/Al/Ca/Al and ITO/PEDOT:PSS/Pd, and was found to be ≈3.68 Ω for electron-only devices and 20.48 Ω for hole-only devices.

Organic Solar Cell Fabrication: OPVs were fabricated using ITO-coated glass substrates (15 Ω sq^{-1}), which were cleaned with detergent, deionized water, acetone, and isopropyl alcohol. A thin layer (≈35 nm) of PEDOT:PSS (Baytron P VP AI 4083, filtered at 0.45 μm) was first spin coated onto the precleaned ITO-coated glass substrates at 5000 rpm and baked at 140 °C for 10 min under ambient conditions. The substrates were then transferred into a nitrogen filled glove box. Subsequently, the donor:$PC_{71}BM$ active layer was spin coated (800 rpm for 2 min) on the PEDOT:PSS layer from a homogeneous solution. The solution was prepared by dissolving the donor and fullerene (1:2 ratio) in *o*-dichlorobenzene at a 10 mg mL^{-1} concentration, which was stirred overnight and filtered through a polytetrafluoroethylene filter (0.45 μm). A fullerene surfactant layer was then spun onto the active layer followed by thermal evaporation of silver (100 nm) under high vacuum (<2 × 10^{-6} Torr) to serve as the cathode. *J–V* curves in this study were recorded using a Keithley 2400 source measure unit. The device photocurrent was measured under illumination from a 450 W Thermal Oriel solar simulator - air mass (AM) 1.5G. The illumination intensity of the light source was accurately calibrated employing a standard Si photodiode detector equipped with a KG-5 filter, which can be traced back to the standard cell of the National Renewable Energy Laboratory (NREL). The calibration method, based on the IEC-69094-1 spectrum, followed procedures described previously. The EQE spectra were obtained by the internal power conversion efficiency measurement using the combination of a Xenon lamp (Oriel, 450 W) as the light source, a monochromator, chopper with frequency of 100 Hz, a lock-in amplifier (SR830, Stanford Research Corp), and a Si-based diode (J115711-1-Si detector) for calibration.

Synthetic Methods: 7-Bromo-5,6-difluoro-4-(5′-hexyl[2,2′-bithiophen]-5-yl)benzo[c][1,2,5]thiadiazole. A solution of 4,7-dibromo-5,6-difluorobenzo[c][1,2,5]thiadiazole (468 mg, 1.42 mmol) and 5′-hexyl-2,2′-bithiophene-5-trimethylstannane (616 mg, 1.49 mmol) in tetrahydrofuran (THF) (20 mL) was deoxygenated by bubbling nitrogen through it for 30 min. $Pd_2(dba)_3$ (26 mg, 2 mol%) and tri(*o*-tolyl)phosphine (34.7 mg, 8 mol%) were added and the mixture was refluxed under nitrogen for 24 h. The mixture was cooled to room temperature and the solvent was removed under reduced pressure. The residue was then purified using silica gel column chromatography, using 7:1 hexane:chloroform as the eluent. Product containing fractions were evaporated and the product was recrystallized from absolute ethanol (to remove benzothiadiazole starting material, which has a similar R_f value to that of the product) to yield orange crystals (41% yield, 290 mg). ^{1}H NMR (500 MHz, $CDCl_3$, δ): 8.12 (d, J = 4 Hz, 1H), 7.26 (d, J = 3.5 Hz, 1H), 7.18 (d, J = 3.5 Hz, 1H), 6.77 (d, J = 3.5 Hz, 1H), 2.85 (t, J = 7.5 Hz, 2H), 1.73 (m, J = 7 Hz, 2H), 1.35–1.43 (br m, 6H), 0.93 (t, 3H); ^{13}C NMR ($CDCl_3$, δ): 153.5, 151.8, 151.3, 149.9, 147.7, 146.8, 142.2, 133.9, 132.5, 132.4, 128.9, 125.1, 124.4, 123.3, 31.6, 31.5, 30.3, 28.8, 22.6, 14.1; ^{19}F NMR ($CDCl_3$, δ): –120.37 (d), –126.90 (d); HRMS (ESI) m/z: $[M+H]^+$ calcd for $C_{20}H_{17}BrF_2N_2S_3$, 498.9778; found, 498.9759.

7-Bromo-6-fluoro-4-(5-hexylthieno[3,2-b]thien-2-yl)benzo[c][1,2,5]thiadiazole: A solution of 4,7-dibromo-5-fluorobenzo[*c*][1,2,5]thiadiazole (500 mg, 1.61 mmol) and trimethyl(5-hexylthieno[3,2-*b*]thien-2-yl) stannane (652 mg, 1.69 mmol) in toluene (23 mL) was deoxygenated by bubbling nitrogen through it for 30 min. $Pd(PPh_3)_4$ (74 mg, 4 mol%) was added and the mixture was heated at 80 °C for 3 d under nitrogen. The solvent was evaporated and the crude product was purified using silica gel column chromatography, eluting with 3:1 hexane:chloroform. After evaporation of the combined product containing fractions, the product was recrystallized from absolute ethanol (to remove benzothiadiazole starting material, which has a similar R_f value to that of the product) to yield yellow crystals (76% yield, 558 mg). ^{1}H NMR (300 MHz, $CDCl_3$, δ): 8.39 (s, 1H), 7.62 (d, J = 10.2 Hz, 1H), 6.97 (s, 1H), 2.93 (t, J = 7.5 Hz, 2H), 1.74 (m, J = 7.2 Hz, 2H), 1.32–1.41 (m, 6H), 0.90 (t, J = 6.9 Hz, 3H); ^{13}C NMR ($CDCl_3$, δ): 161.7, 159.7, 154.3, 151.4, 148.8, 140.3, 138.5, 137.0, 128.1, 122.4, 116.4, 115.6, 31.6, 31.4, 31.3, 28.8, 22.6, 14.1; ^{19}F NMR ($CDCl_3$, δ): -104.38 (d); HRMS (ESI) m/z: $[M+H]^+$ calcd for $C_{18}H_{16}BrFN_2S_3$, 454.9716; found, 454.9706.

7-Bromo-6-fluoro-4-(5″-hexyl[2,2′:5′,2″-terthiophen]-5-yl)benzo[c][1,2,5]thiadiazole: This compound was made using the same procedure as the thienothiophene derivative given above, using (5″-hexyl[2,2′:5′,2″-terthiophen]-5-yl)trimethylstannane. The product was obtained as a red solid (74% yield). ^{1}H NMR (500 MHz, $CDCl_3$, δ): 8.02 (d, J = 3.9 Hz, 1H), 7.67 (d, J = 10 Hz, 1H), 7.21 (d, J = 3.85 Hz, 1H), 7.17 (d, J = 3.7 Hz, 1H), 7.02 (d, J = 3.7 Hz, 1H), 7.00 (d, J = 3.4 Hz, 1H), 6.70 (d, J = 2.75 Hz, 1H), 2.80 (t, J = 7.4 Hz, 2H), 1.69 (m, J = 7.5 Hz, 2H), 1.32–1.39 (br m, 6H), 0.90 (t, J = 5.9 Hz, 3H); ^{13}C NMR ($CDCl_3$, δ): 161.7, 159.7, 148.8, 146.1, 140.4, 138.0, 135.5, 134.6, 134.2, 129.9, 127.1, 125.1, 124.9, 124.3, 123.7, 123.6, 115.5, 115.3, 31.6, 31.5, 30.2, 28.8, 22.6, 14.1. ^{19}F NMR ($CDCl_3$, δ): –104.38 (d); HRMS (ESI) m/z: $[M]^{\cdot+}$ calcd for $C_{20}H_{16}BrF_2N_2S_3$, 561.9671; found, 561.9660.

General Procedure for the Synthesis of IDTT-Based Molecules: A solution of 6,6,12,12-tetrakis(4-hexylphenyl)-s-indacenodithieno[3,2-b]thiophene-bis(trimethylstannane) (0.10 mmol) and the corresponding

bromobenzothiadiazole-oligiothiophene (0.23 mmol) in THF (5 mL) was deoxygenated by bubbling nitrogen through it for 30 min. $Pd_2(dba)_3$ (1.8 mg, 2 mol%) and tri(*o*-tolyl)phosphine (2.4 mg, 8 mol%) were added and the mixture was refluxed under nitrogen for 3 d. The solution was cooled and the solvent was evaporated off. The crude product was purified on a silica gel column three times using a hexane/chloroform gradient to ensure the purity of the material. The product was then dissolved in chloroform and precipitated into acetone and the resulting solid was collected and dried under vacuum.

IDTT-DFBT-BT: (68% yield) ^{1}H NMR (500 MHz, $CDCl_3$, δ): 8.66 (s, 2H), 8.20 (d, J = 3.9 Hz, 2H), 7.58 (s, 2H), 7.22–7.28 (br m, 10H), 7.12–7.15 (br m, 10H), 6.73 (d, J = 3.6 Hz, 2H), 2.82 (t, J = 7.6 Hz, 4H), 2.57 (t, J = 7.9 Hz, 8H), 1.71 (m, J = 7.6 Hz, 4H), 1.60 (m, J = 7.8 Hz, 8H), 1.22–1.35 (br m, 36H), 0.84–0.92 (br m, 18H); HRMS (ESI) m/z: $[M]^{2\cdot2+}$ calcd for $C_{108}H_{106}F_4N_4S_{10}$, 927.7792; found, 927.7765; Anal. Calcd: C, 69.9; H, 5.8; N, 3.0; found: C, 69.8; H, 5.9, 2.6.

IDTT-FBT-TT: (66% Yield) ^{1}H NMR (500 MHz, $CDCl_3$, δ): 8.64 (s, 2H), 8.42 (s, 2H), 7.70 (d, J = 13 Hz, 2H), 7.56 (s, 2H), 7.27 (br m, 8H), 7.13 (d, J = 8 Hz, 8H), 7.00 (s, 2H), 2.92 (t, J = 7.5 Hz, 4H), 2.57 (t, J = 8 Hz, 8H), 1.75 (m, J = 7.5 Hz, 4H), 1.60 (m, J = 7 Hz, 8H), 1.27–1.42 (br m, 36H), 0.82–0.93 (br m, 18H); HRMS (ESI) m/z: $[M]^{\cdot+}$ calcd for $C_{104}H_{104}F_2N_4S_{10}$, 1767.5464; found, 1767.5400; Anal. Calcd: C, 70.6; H, 5.9; N, 3.2; found: C, 70.2; H, 5.8, N, 2.9.

IDTT-FBT-BT: (70% yield) ^{1}H NMR (500 MHz, $CDCl_3$, δ): 8.63 (s, 2H), 8.01 (d, J = 4 Hz, 2H), 7.68 (d, J = 13.5 Hz, 2H), 7.57 (s, 2H), 7.28 (d, J = 8 Hz, 8H), 7.17 (d, J = 4 Hz, 2H), 7.13 (d, J = 8.5 Hz, 8H), 7.11 (d, J = 3.5 Hz, 2H), 6.72 (d, J = 3.5 Hz, 2H), 2.81 (t, J = 7.5 Hz, 4H), 2.57 (t, J = 8 Hz, 8H), 1.70 (m, J = 7.5 Hz, 4H), 1.60 (m, J = 8 Hz, 8H), 1.28–1.34 (br m, 36H), 0.85–0.93 (br m, 18H); HRMS (ESI) m/z: $[M]^{2\cdot2+}$ calcd for $C_{108}H_{108}F_2N_4S_{10}$, 909.7886; found, 909.7855; Anal. Calcd: C, 71.3; H, 6.0, N; 3.1; found: C, 71.2; H, 5.7; N, 2.9.

IDTT-FBT-3T: (70% yield) ^{1}H NMR (500 MHz, $CDCl_3$, δ): 8.67 (s, 2H), 8.05 (d, J = 4 Hz, 2H), 7.74 (d, J = 13 Hz, 2H), 7.59 (s, 2H), 7.30 (d, J = 8 Hz, 8H), 7.26 (d, J = 3.5 Hz, 2H), 7.21 (d, J = 3.5 Hz, 2H), 7.16 (d, J = 8.5 Hz, 8H), 7.06 (d, J = 3.5 Hz, 2H), 7.03 (d, J = 3.5 Hz, 2H), 6.72 (d, J = 3 Hz, 2H), 2.83 (t, J = 7.5 Hz, 4H), 2.60 (t, J = 8 Hz, 8H), 1.71 (m, J = 7.5 Hz, 4H), 1.62 (m, J = 8 Hz, 8H), 1.30–1.42 (br m, 36H), 0.86–0.94 (br m, 18H); HRMS (ESI) m/z: $[M]^{2\cdot2+}$ calcd for $C_{108}H_{108}F_2N_4S_{10}$, 991.7763; found, 991.7739; Anal. Calcd: C, 70.2; H, 5.7; N, 2.8; found: C, 69.9; H, 5.7; N, 2.6.

Supporting Information

Supporting Information is available from the Wiley Online Library or from the author.

Acknowledgements

The authors thank the support from the National Science Foundation (DMR-0120967), the Air Force Office of Scientific Research (FA9550-09-1-0426), the Asian Office of Aerospace R&D (FA2386-11-1-4072), and the Office of Naval Research (N00014-11-1-0300). A.K.-Y.J. thanks the Boeing Foundation for support.

Received: April 21, 2015
Revised: June 3, 2015
Published online: July 2, 2015

[1] a) B. Kan, Q. Zhang, M. Li, X. Wan, W. Ni, G. Long, Y. Wang, X. Yang, H. Feng, Y. Chen, *J. Am. Chem. Soc.* **2014**, *136*, 15529; b) B. Kan, M. Li, Q. Zhang, F. Liu, X. Wan, Y. Wang, W. Ni, G. Long, X. Yang, H. Feng, Y. Zuo, M. Zhang, F. Huang, Y. Cao, T. P. Russell, Y. Chen, *J. Am. Chem. Soc.* **2015**, *137*, 3886.

[2] Y. Liu, C.-C. Chen, Z. Hong, J. Gao, Y. Yang, H. Zhou, L. Dou, G. Li, *Sci. Rep.* **2013**, DOI: 10.1038/srep03356.

[3] H. Zhou, Y. Zhang, C.-K. Mai, S. D. Collins, T.-Q. Nguyen, G. C. Bazan, A. J. Heeger, *Adv. Mater.* **2014**, *26*, 780.

[4] a) T. S. van der Poll, J. A. Love, T.-Q. Nguyen, G. C. Bazan, *Adv. Mater.* **2012**, *24*, 3646; b) N. D. Eisenmenger, G. M. Su, G. C. Welch, C. J. Takacs, G. C. Bazan, E. J. Kramer, M. L. Chabinyc, *Chem. Mater.* **2013**, *25*, 1688.

[5] J. A. Love, C. M. Proctor, J. Liu, C. J. Takacs, A. Sharenko, T. S. van der Poll, A. J. Heeger, G. C. Bazan, T.-Q. Nguyen, *Adv. Funct. Mater.* **2013**, *23*, 5019.

[6] a) J. J. Intemann, K. Yao, H.-L. Yip, Y.-X. Xu, Y.-X. Li, P.-W. Liang, F.-Z. Ding, X. Li, A. K. Y. Jen, *Chem. Mater.* **2013**, *25*, 3188; b) Y.-X. Xu, C.-C. Chueh, H.-L. Yip, C.-Y. Chang, P.-W. Liang, J. Intemann, W.-C. Chen, A. Jen, *Polym. Chem.* **2013**, *4*, 5220; c) I. McCulloch, R. S. Ashraf, L. Biniek, H. Bronstein, C. Combe, J. E. Donaghey, D. I. James, C. B. Nielsen, B. C. Schroeder, W. Zhang, *Acc. Chem. Res.* **2012**, *45*, 714; d) J. J. Intemann, K. Yao, Y.-X. Li, H.-L. Yip, Y.-X. Xu, P.-W. Liang, C.-C. Chueh, F.-Z. Ding, X. Yang, X. Li, Y. Chen, A. K. Y. Jen, *Adv. Funct. Mater.* **2014**, *24*, 1465; e) Y. Zhang, J. Zou, H.-L. Yip, K.-S. Chen, D. F. Zeigler, Y. Sun, A. K. Y. Jen, *Chem. Mater.* **2011**, *23*, 2289; f) H. Bronstein, R. S. Ashraf, Y. Kim, A. J. P. White, T. Anthopoulos, K. Song, D. James, W. Zhang, I. McCulloch, *Macromol. Rapid Commun.* **2011**, *32*, 1664; g) Y.-L. Chen, C.-Y. Chang, Y.-J. Cheng, C.-S. Hsu, *Chem. Mater.* **2012**, *24*, 3964; h) Y. Zhang, J. Zou, H.-L. Yip, K.-S. Chen, J. A. Davies, Y. Sun, A. K. Y. Jen, *Macromolecules* **2011**, *44*, 4752.

[7] W. Yong, M. Zhang, X. Xin, Z. Li, Y. Wu, X. Guo, Z. Yang, J. Hou, *J. Mater. Chem. A* **2013**, *1*, 14214.

[8] X. Guo, M. Zhang, J. Tan, S. Zhang, L. Huo, W. Hu, Y. Li, J. Hou, *Adv. Mater.* **2012**, *24*, 6536.

[9] a) Y.-X. Xu, C.-C. Chueh, H.-L. Yip, F.-Z. Ding, Y.-X. Li, C.-Z. Li, X. Li, W.-C. Chen, A. K. Y. Jen, *Adv. Mater.* **2012**, *24*, 6356; b) H.-H. Chang, C.-E. Tsai, Y.-Y. Lai, D.-Y. Chiou, S.-L. Hsu, C.-S. Hsu, Y.-J. Cheng, *Macromolecules* **2012**, *45*, 9282.

[10] Y. Zhang, S.-C. Chien, K.-S. Chen, H.-L. Yip, Y. Sun, J. A. Davies, F.-C. Chen, A. K. Y. Jen, *Chem. Commun.* **2011**, *47*, 11026.

[11] Y. Li, J. Zou, H.-L. Yip, C.-Z. Li, Y. Zhang, C.-C. Chueh, J. Intemann, Y. Xu, P.-W. Liang, Y. Chen, A. K. Y. Jen, *Macromolecules* **2013**, *46*, 5497.

[12] a) W. J. Potscavage, S. Yoo, B. Kippelen, *Appl. Phys. Lett.* **2008**, *93*, 193308; b) W. J. Potscavage, A. Sharma, B. Kippelen, *Acc. Chem. Res.* **2009**, *42*, 1758.

[13] a) H. Ma, H.-L. Yip, F. Huang, A. K. Y. Jen, *Adv. Funct. Mater.* **2010**, *20*, 1371; b) B. Qi, J. Wang, *J. Mater. Chem.* **2012**, *22*, 24315.

[14] a) O. Tal, Y. Rosenwaks, Y. Preezant, N. Tessler, C. K. Chan, A. Kahn, *Phys. Rev. Lett.* **2005**, *95*, 256405; b) I. N. Hulea, H. B. Brom, A. J. Houtepen, D. Vanmaekelbergh, J. J. Kelly, E. A. Meulenkamp, *Phys. Rev. Lett.* **2004**, *93*, 166601; c) T. Sueyoshi, H. Fukagawa, M. Ono, S. Kera, N. Ueno, *Appl. Phys. Lett.* **2009**, *95*, 183303.

[15] a) B. Yang, Y. Yuan, P. Sharma, S. Poddar, R. Korlacki, S. Ducharme, A. Gruverman, R. Saraf, J. Huang, *Adv. Mater.* **2012**, *24*, 1455; b) L. J. A. Koster, S. E. Shaheen, J. C. Hummelen, *Adv. Energy Mater.* **2012**, *2*, 1246.

[16] a) S. Ko, E. T. Hoke, L. Pandey, S. Hong, R. Mondal, C. Risko, Y. Yi, R. Noriega, M. D. McGehee, J.-L. Brédas, A. Salleo, Z. Bao, *J. Am. Chem. Soc.* **2012**, *134*, 5222; b) K. R. Graham, P. Erwin, D. Nordlund, K. Vandewal, R. Li, G. O. N. Ndjawa, E. T. Hoke, A. Salleo, M. E. Thompson, M. D. McGehee, A. Amassian, *Adv. Mater.* **2013**, *25*, 6076; c) C. W. Schlenker, M. E. Thompson, *Chem. Commun.* **2011**, *47*, 3702.

[17] C.-Z. Li, H.-L. Yip, A. K. Y. Jen, *J. Mater. Chem.* **2012**, *22*, 4161.

[18] a) C. J. Takacs, Y. Sun, G. C. Welch, L. A. Perez, X. Liu, W. Wen, G. C. Bazan, A. J. Heeger, *J. Am. Chem. Soc.* **2012**, *134*, 16597; b) J. E. Coughlin, Z. B. Henson, G. C. Welch, G. C. Bazan, *Acc. Chem. Res.* **2013**, *47*, 257.

[19] J. C. Blakesley, D. Neher, *Phys. Rev. B: Condens. Matter Mater. Phys.* **2011**, *84*, 075210.
[20] G. Garcia-Belmonte, P. P. Boix, J. Bisquert, M. Lenes, H. J. Bolink, A. La Rosa, S. Filippone, N. Martín, *J. Phys. Chem. Lett.* **2010**, *1*, 2566.
[21] K. Celebi, P. J. Jadhav, K. M. Milaninia, M. Bora, M. A. Baldo, *Appl. Phys. Lett.* **2008**, *93*, 083308.
[22] a) K. S. Nalwa, J. A. Carr, R. C. Mahadevapuram, H. K. Kodali, S. Bose, Y. Chen, J. W. Petrich, B. Ganapathysubramanian, S. Chaudhary, *Energy Environ. Sci.* **2012**, *5*, 7042; b) Y. Zhang, H. Zhou, J. Seifter, L. Ying, A. Mikhailovsky, A. J. Heeger, G. C. Bazan, T.-Q. Nguyen, *Adv. Mater.* **2013**, *25*, 7038.
[23] N. Cho, C. W. Schlenker, K. M. Knesting, P. Koelsch, H.-L. Yip, D. S. Ginger, A. K. Y. Jen, *Adv. Energy Mater.* **2014**, *4*, 1301857.
[24] C.-Y. Yu, B.-T. Ko, C. Ting, C.-P. Chen, *Sol. Energy Mater. Sol. Cells* **2009**, *93*, 613.
[25] Z. B. Henson, G. C. Welch, T. van der Poll, G. C. Bazan, *J. Am. Chem. Soc.* **2012**, *134*, 3766.
[26] J. Huang, H. Jia, L. Li, Z. Lu, W. Zhang, W. He, B. Jiang, A. Tang, Z. Tan, C. Zhan, Y. Li, J. Yao, *Phys. Chem. Chem. Phys.* **2012**, *14*, 14238.